buildings

Article

Design Optimization of a Hybrid Vibration Control System for Buildings

Basel Salaas [1], Gebrail Bekdaş [1,*], Yasser E. Ibrahim [2], Sinan Melih Nigdeli [1], Mohamed Ezzat [2], Mahmoud Nawar [2,*] and Aylin Ece Kayabekir [3]

1 Department of Civil Engineering, Faculty of Engineering, Istanbul University-Cerrahpaşa, İstanbul 34320, Turkey
2 Engineering Management Department, College of Engineering, Prince Sultan University, Riyadh 12435, Saudi Arabia
3 Department of Civil Engineering, Faculty of Engineering, Istanbul Gelişim University, İstanbul 34320, Turkey
* Correspondence: bekdas@iuc.edu.tr (G.B.); mnawar@psu.edu.sa (M.N.)

Abstract: Control of high-rise structures under seismic excitations was investigated using a passive hybrid control system consisting of a base-isolation (BI) subsystem and a passive tuned liquid column damper (TLCD) system. Both of the systems were optimized considering using the other system in the same structure. An optimization method was developed, and a computer code was written based on dynamic analysis of the structure and metaheuristic optimization methods. Within the scope of the study, a general solution was found by using many earthquake records during the optimization process. Moreover, one of the most suitable and successful metaheuristic algorithms was used in this study. In addition, numerical simulations were performed on a benchmark high-rise building structure to investigate the effectiveness of the optimized hybrid control system in controlling the seismic response of the building. The performance of the base-isolated TLCD-controlled structure was examined when the TLCD was placed on the base floor by using a set of 44 recorded ground motions as base excitations. Based on the results obtained from this study, the use of a base-isolation subsystem decoupling the superstructure from the ground motions by lowering the structure's fundamental natural frequency reduces the structural responses of the building in most cases. The responses of the base-isolation subsystem were not too large since the parameters of the BI subsystem were optimized specifically for the investigated structure. Nevertheless, displacements of BI might exceed the maximum limit to undesirable values in some cases. The TLCD system appears to be quite effective in protecting the base-isolation subsystem by reducing its displacements to the maximum allowable limit or below when attached to it. Moreover, the proposed passive hybrid control system can effectively reduce the structural responses under seismic excitations.

Keywords: base-isolated building; TLCD; optimal design; hybrid control; metaheuristic algorithms; JAYA algorithm

Citation: Salaas, B.; Bekdaş, G.; Ibrahim, Y.E.; Nigdeli, S.M.; Ezzat, M.; Nawar, M.; Kayabekir, A.E. Design Optimization of a Hybrid Vibration Control System for Buildings. *Buildings* **2023**, *13*, 934. https://doi.org/10.3390/buildings13040934

Academic Editors: Chunfeng Zhao, Xiaohui Yu and Wen Bai

Received: 10 February 2023
Revised: 21 March 2023
Accepted: 28 March 2023
Published: 1 April 2023

1. Introduction

Earthquakes are considered among nature's most dangerous hazards that occur suddenly and are unpredictable. Some earthquakes are huge and destructive, leading to catastrophes. There are approximately 11,000 deaths reported every year due to earthquakes. The massive damaging potential of an earthquake can also cause major damage to structures and the contents of structures. Apart from the loss of lives, there is also an impact on the economy of countries due to damage to properties [1].

For instance, on 12 May 2008, China experienced the Wenchuan earthquake on the eastern edge of the Tibetan Plateau with a magnitude of 7.9 which resulted in more than 17,000 deaths, 374,643 injuries, and the destruction of many buildings [2]. On 12 January 2010, Haiti experienced the greatest earthquake ever recorded in the country with a magnitude of 7.0. It was centered 15 miles southwest of Port-au-Prince. According to experts, the overall damage costs were approximately USD 8 to USD 14 billion. Three million people (approximately one-third of the population) were affected. According to government reports, 230,000 people died and 300,600 were injured. Almost all buildings in the country were damaged or collapsed [3].

Engineers are working hard to come up with solutions to prevent or keep the impact of earthquakes to a minimum. The main challenge for structural engineers is to reduce the impact of earthquakes on buildings. One of the effective strategies for protecting structures from earthquake effects and for obtaining the desired performance is to reduce the seismic demand on the system [4].

Conventionally, the seismic impact design approach was based on increasing the strength or ductility of the building. This leads to an increase in the stiffness of the structure resulting in higher floor accelerations, which causes damage to building contents. Previous earthquakes have shown that structures collapse or become dysfunctional when the ductility capacity of the structure is consumed. Even in cases where the building has been designed with more strength and ductility, vibration-sensitive equipment in the structure may lose function due to high accelerations. In order to keep such equipment functional after an earthquake, engineers have adopted an alternative approach called seismic isolation [5].

The aim of seismic isolation is to reduce seismic demand instead of increasing the capacity of the structure. Introducing a flexible interface between the foundation and the base of the structure in seismically base-isolated systems decouples the superstructure from the earthquake ground motion. Earthquakes generally contain low-period or high-frequency waves. To protect the structure from damage, the isolation system increases the dominant period of the structure in order to decouple it from the ground-dominant shaking period. During an earthquake, an isolation system preserves structural integrity by making large displacements and by expending earthquake energy through damping, resulting in reduced floor accelerations and relative floor displacements in the superstructure [6].

If the fixed-base fundamental frequency of the structure is significantly higher than that of the base-isolated system, the first mode of the base-isolated structure is mainly a rigid body mode with all displacement in the rubber of the base. The second mode's frequency is between 50% and 100% higher than the fixed-base frequency. It is possible to consider the magnitude of the seismic input as an equivalent lateral force proportional to the rigid body mode. All modes greater than the first will be orthogonal to the input motion because a linear vibrating system has the property that all modes are mutually orthogonal, so if there are high energies in the earthquake ground movement at the frequencies of these higher modes, this energy cannot be transmitted into the building [7].

Because most of the displacement is on the base-isolation subsystem, the structure acts like a rigid body, and this leads to a great reduction in the structure's displacements and accelerations. However, there might be significant, occasionally unwanted, displacements in the base-isolation subsystem. Increasing the damping in the isolation system leads to a reduction in the isolator displacement and structural base shear; however, the floor acceleration and the interstory drift are increased, resulting in a negative effect on the structure [8].

In order to facilitate these displacements at the base-isolation level and avoid poundings with the adjacent moat wall, a seismic gap must be given as a clearance around the building. The size of the available gap has a big impact on how a base-isolated building reacts to earthquakes. Low seismic gap sizes require us to select base-isolators that are fairly stiff in order to prevent significant horizontal base displacements, which result in relatively high values of floor acceleration. More flexible base-isolators must be used in order to achieve low floor acceleration values, but this also demands a large seismic gap to handle the resulting horizontal base displacements. Moreover, when the peak ground acceleration (PGA) scaling values are increased, the necessary gap becomes noticeably bigger. Interstory seismic isolators with appropriate stiffness values were introduced at higher elevations in [9,10] to avoid the problems encountered with base slab displacements due to the narrow seismic gaps specified. The main benefit of interstory seismic isolation is the interruption of the energy flow between the upper and lower stories, which has made it a valuable solution for high-rise buildings to effectively separate the various parts having multiple functions [11].

Several research efforts resorted to many different strategies to lower the base-isolation subsystem's displacement range. Previous research concluded that coupling the base-isolated structures with passive, active, or semi-active devices can make the base isolator more efficient. In [12], researchers aimed to reduce the absolute base displacement by combining a class of passive nonlinear base isolators with an active control system. One step forward, other researchers proposed a passive hybrid control that comprised the coupling of a base isolator and a tuned mass damper (TMD) [13]. Shape memory alloy (SMA)-based friction pendulum bearings (FPBs) were proposed in order to control a three-span continuous isolated bridge [14]. A multi-stage super-elastic variable stiffness pendulum isolator (SVSPI) was generated by hybridizing of super-elastic shape memory alloy (SMA) and the multi-stage variable stiffness pendulum isolator (VSPI) in order to effectively adapt the system under service conditions and near-fault excitations [15].

For the first time, Hochrainer and Ziegler [16] used TLCD, another type of passive control system to control a five-story base-isolated building. The typical model for TLCD is an SDOF system that is rigidly attached to a vibrating structure [17–19]. Like with a TMD, its effectiveness is dependent on the right tuning of the natural frequency and damping ratio. However, contrary to the typical TMD, the TLCD response is nonlinear, making it impossible to determine the ideal damping parameters a priori without first knowing the value of the force [17].

Metaheuristics have been successfully applied to TMD as a numerical optimization method, including the members of this study [20–22]; however, an exact optimization using metaheuristics has not been proposed for the optimization of TLCD positioned on base-isolated structures. The challenge is in the need to consider the properties of both base isolators and TLCD as design variables. In this regard and based on a dynamic analysis of the structure and metaheuristic optimization techniques, an optimization method was created, and a computer code was constructed. During the optimization phase, a generic solution was identified using multiple earthquake records. In addition, one of the most effective metaheuristic algorithms was applied. In order to determine how well the optimized hybrid control system controls the building's seismic response, numerical simulations of a benchmark high-rise building structure were also run. The performance of the base-isolated TLCD-controlled structure was evaluated by using 44 recorded ground vibrations as base excitations for the case of attaching the TLCD to the base level.

The objective of this study is to develop a method to optimize the design of vibration control systems to ensure the safety of people, buildings, and infrastructure during seismic excitations and to prevent huge losses in the economic resources and capabilities of countries. These control systems operate to dissipate the vibrations by decreasing the response of structures exposed to ground excitations and winds. Aside from safety insurance, it also raises the standard of living for people who live or work in high-rise towers by not being exposed to the feeling of the vibrations caused by wind actions. In this regard, the control of high-rise building structures under seismic excitations was investigated by using a passive hybrid control system composed of a passive tuned liquid column damper system and base-isolation subsystem. Both of the systems were specifically optimized considering using the other system in a structure subject to earthquake effects. As a novelty, the paper includes the optimization of the design parameter of two control systems, including the geometric dimensions of TLCD via metaheuristic algorithms.

2. Seismic Isolation

2.1. Principle of Seismic Isolation

Seismic isolation aims to reduce seismic demand rather than increase the capacity of the structure. A flexible structural system from an earthquake resistance viewpoint is created by matching the fundamental frequencies of base-isolated structures and the predominant frequency contents of earthquakes [23].

Seismic isolation technology is highly preferred, especially in strategic buildings where sensitive equipment is intended to be protected from hazardous effects during earthquakes, such as schools, hospitals, and industrial structures [24]. Seismic isolated structures' performance is generally evaluated by base displacements, base and floor accelerations, and relative floor displacements [6].

Although a properly designed seismic isolation system reduces floor accelerations and relative floor displacements to acceptable limits in far-fault earthquakes without causing unacceptably large displacements, the effectiveness of an isolation system in near-fault earthquakes is questionable due to its potential for very large isolator displacements [25].

2.2. Types of Seismic Isolation

In general, seismic isolation systems can be grouped into two main categories: elastomeric-based systems and friction-based systems. As technology develops, different isolation systems emerge, but these new systems must satisfy the fundamental requirements explained in [26].

3. Tuned Liquid Column Damper (TLCD)

TLCD is an innovative absorber that depends on the motion of an oscillating liquid column inside a container which counteracts external motion, while a built-in orifice plate induces turbulent damping forces that dissipate kinetic energy and structural vibrations.

3.1. Geometry of TLCD

The literature [27] has proposed various TLCD geometries. The U-shaped container, which consists of one horizontal and two vertical water-filled pipes, is the most widely used [28]. Figure 1 illustrates B and H, which demonstrate the liquid columns' inclined and horizontal lengths, respectively, and whose cross-sectional areas AB and AH are assumed to be constant. The displacement, u1 = u2 = u(t), describes the liquid column's relative motion.

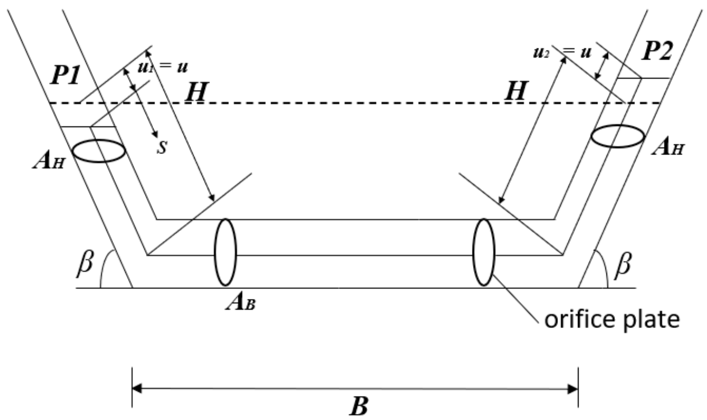

Figure 1. Tuned liquid column damper geometry.

3.2. Modeling of TLCD

3.2.1. The Equation of Relative Motion of TLCD to Reduce Single-Direction Vibration

The Equation (1) of motion is obtained by integrating along the relative streamline. The uniaxial floor or ground acceleration is provided by $\ddot{w}_g$, see Figure 1 [29],

$$\begin{gathered} \ddot{u} + \frac{\Delta p_L}{\rho L_{eff}} + \frac{\Delta p}{\rho L_{eff}} + \omega_A^2 u = -k(\ddot{w}_g + \ddot{w}), \\ \Delta p = p_2 - p_1, \\ \Delta p_L = \frac{\rho|\dot{u}|u}{2}\lambda(Re), \end{gathered} \tag{1}$$

where ρ, Δp, and Δp_L designate the density of a liquid, e.g., of water ρ = 1000 kg/m^3, the streamlined pressure loss, and the pressure difference. Δp_L is a product of the loss factor $\lambda(Re)$, a function of the Reynolds number $Re = 2R\frac{\dot{u}}{v}$, and the stagnation pressure $\frac{\rho|\dot{u}|u}{2}$. The kinematic viscosity is denoted by the letter v, and R is a typical cross-sectional size. The effective length L_{eff} of the liquid column and the geometry-dependent excitation influence factors k, where $\ddot{w}$ is the floor's relative horizontal displacement. All this is defined by,

$$\begin{aligned} k &= \frac{B + 2Hcos\beta}{L_{eff}}, \\ L_{eff} &= 2H + \frac{A_H}{A_B}B, \end{aligned} \tag{2}$$

The TLCD's undamped linear natural circular frequency can be calculated using,

$$\omega_A = \sqrt{\frac{2gsin\beta}{L_{eff}}}, \tag{3}$$

where g stands for the gravitational constant, g = 9.81 m/**s**^{2}. The air pressure at the free surfaces is about equal to the ambient pressure $p_1 = p_2 = p_0$, and the pressure differential Δp vanishes when the nonlinear damping factor $\frac{\Delta p_L}{\rho L_{eff}}$ is replaced by its viscous counterpart $2\xi_A\omega_A\dot{u}$.

To connect the TLCD with the main structure, it is crucial to understand the interface responses. Only the interaction forces between the massless, rigid, liquid-filled system and the supporting floor are considered, assuming that the floor mass has been increased by the dead weight of a rigid piping system (at this point, dead fluid mass is not considered). The reaction forces acting on the supporting floor are,

$$\begin{aligned} F_x &= -m_f(\ddot{w}_g + \underline{k}\ddot{u}), \\ \underline{k} &= kL_{eff}/L_1, \\ L_1 &= 2H + \frac{A_B}{A_H}B, \end{aligned} \tag{4}$$

where $m_f = \rho A_H L_1$ designates the total fluid mass.

3.2.2. The Equation of Relative Motion of TLCD to Reduce Coupled Translation and Rotation Vibrations

When a TLCD is implemented, its direction in the floor of an asymmetrical structure is directed by the reference point A $(y_A, z_A, 0)$ and the angle γ to the y-direction. The generalized nonstationary method, the Bernoulli equation, is used to construct the optimal fluid flow equation for rigid pipe systems [30],

$$\begin{aligned} &\ddot{u} + 2\xi_A\omega_A\dot{u} + \omega_A^2 u \\ &= -k\left\{\left[\ddot{v}_g + \ddot{v} - (z_A - z_{C_M})\ddot{\theta}\right]cos\gamma + \left[\ddot{w}_g + \ddot{w} + (y_A - y_{C_M})\ddot{\theta}\right]sin\gamma\right\}, \end{aligned} \tag{5}$$

In y, z, and θ directions, the control forces F_{Ay}, F_{AZ}, and M_A are determined by using the momentum and angular momentum of the moving fluid,

$$
\begin{gathered}
F_{Ay} = m_f\left[\ddot{v}_g + \ddot{v} - \frac{(z_A - z_{C_M})\ddot{u}_T}{r_S}\right] + \underline{k}m_f\ddot{u}cos\gamma, \\
F_{Az} = m_f\left[\ddot{w}_g + \ddot{w} - \frac{(y_A - y_{C_M})\ddot{u}_T}{r_S}\right] + \underline{k}m_f\ddot{u}sin\gamma, \\
u_T = \theta r_S, \\
M_{Ax} = m_f\underline{k}_3H^2\ddot{\theta}, \\
\underline{k}_3 = \frac{2H}{L_1}[\left(\frac{B}{2H}\right)^2 + \frac{A_B}{3A_H}\left(\frac{B}{2H}\right)^3 + \frac{B}{2H}cos\beta + \frac{1}{3}cos^2\beta],
\end{gathered} \tag{6}
$$

and the linearized moment M_x is determined by,

$$
M_x = M_{Ax} - F_{Ay}(z_A - z_M) + F_{Az}(y_A - y_M), \tag{7}
$$

4. Approximate Substructure Synthesis

Recently, there has been an increasing interest in applying TLCDs as a solution for the vibration reduction of structures [31]. Proper tuning and damping values determine the impact of TLCD's damping on controlling structural vibrations. Taking advantage of the proposed approximated formulation in [17], the ideal TLCD parameters can be calculated by a smooth function that can be formed and easily minimized and defines the primary system variance. Since neither the random vibration theory nor modern control theory can provide a similar design statement of TMD, the real TLCD design is cumbersome. The TLCD damping effect simulation in MATLAB for a non-standard structure is too complicated. An equivalent computation approach was put out by [32], providing a plausible process of transformation for controlling the structural vibration of a tuned liquid damper with a clear physical meaning (TMD-structure to TLD-structure system). The approach of converting the TLCD-structure system into the TMD-structure system was utilized in [33] to examine parameter optimization and numerical calculation, and Den Hartog's method was employed to optimize the TLCD's parameters. In this study, proceeding from the method of transformation used in [33], an optimization method was developed, and a computer code was written based on dynamic analysis of the structure and metaheuristic optimization methods in order to come out with an optimum design for the TLCD and BI systems.

4.1. The Symmetric Structure with TLCD/TMD

For an implemented TLCD on a floor that is propelled by base excitation $\vec{\ddot{w}}_g$ and wind forces $\vec{F}(t)$, the following equation of motion determines how the TLCD and the main structure interact,

$$
\begin{gathered}
\tilde{M}\vec{\ddot{w}} + \tilde{C}\vec{\dot{w}} + \tilde{K}\vec{w} = -\tilde{M}\vec{\ddot{w}}_g + \vec{F}(t) + \vec{s}F_z, \\
\vec{s} = [0, \ldots, 1, \ldots, 0],
\end{gathered} \tag{8}
$$

where $\tilde{M}$ is the diagonal mass matrix. The primary system's light damping and stiffness matrices are $\tilde{C}$ and $\tilde{K}$, respectively; $\vec{w}$ is the floor displacement.

The primary system is changed when the "equivalent" tuned mechanical damper TMD is used in place of the TLCD; the parameters are indicated by an asterisk,

$$
\begin{gathered}
\tilde{M}^*\vec{\ddot{w}} + \tilde{C}^*\vec{\dot{w}} + \tilde{K}^*\vec{w} = -\tilde{M}^* r_s\vec{\ddot{w}}_g + \vec{F}(t) + \vec{s}F^*{}_z, \\
\text{Control force}: \; F^*{}_z = -m^*{}_A(\ddot{w}_g + \vec{s}^T\vec{\ddot{w}} + \ddot{u}^*),
\end{gathered} \tag{9}
$$

$$
\ddot{u}^* + 2\xi_A{}^*\omega_A{}^*\dot{u}^* + \omega_A{}^{*2}u^* = -(\ddot{w}_g + \vec{s}^T\vec{\ddot{w}}), \tag{10}
$$

The fact that the TMD behavior can be inferred from the corresponding TLCD by setting $k = \underline{k} = 1$ is a strong hint that a similarity exists.

4.2. The Asymmetric Structure with TLCD/TMD

On the level i of an N-story plan-asymmetric space frame, a single TLCD is installed with a general angle γ to y-direction and a reference point of $A\ (y_A, z_A, 0)$. With the use of an oblique single-point base excitation $\ddot{\vec{x}}_g^{\,T} = [\ddot{v}_g\ \ddot{w}_g\ 0]$ and by wind forces $\vec{F}(t)$, the equation of motion for the main system may be expressed as a hypermatrix,

$$\begin{gathered}
\widetilde{M}\ddot{\vec{x}} + \widetilde{C}\dot{\vec{x}} + \widetilde{K}\vec{x} = -\widetilde{M}\ddot{\vec{x}}_{gN} + \vec{F}(t) + \vec{F}_A,\ \vec{x}^{\,T} = [\vec{x}_1^{\,T} \ldots \vec{x}_i^{\,T} \ldots \vec{x}_N^{\,T}], \\
\vec{x}_i^{\,T} = [v_i\ w_i\ u_{Ti}],\ u_{Ti} = \theta_i r_{Si},\ \ddot{\vec{x}}_{gN} = \widetilde{E}_N \ddot{\vec{x}}_g, \\
\widetilde{E}_N = [1\,0\,0\,1\,0\,0\,1 \ldots\ 0\,1\,0\,0\,1\,0\,0 \ldots 0\,0\,0\,0\,0\,0\,0 \ldots]^T, \\
\widetilde{M} = diag[\widetilde{M}_1 \ldots \widetilde{M}_i \ldots \widetilde{M}_N] = 3N \times 3N, \\
\vec{F}_A^{\,T} = \left[0, \ldots, F_{Aiy}, F_{Aiz}, \frac{M_{xi}}{r_{si}}, \ldots, 0\right],
\end{gathered} \tag{11}$$

Equation (12) is produced by the standard analysis when the passive spring-mass damper is taken into account in the same location on the same floor connected. Referring to TMD, an asterisk is used to indicate every parameter,

$$\begin{gathered}
\widetilde{M}^*\ddot{\vec{x}} + \widetilde{K}^*\vec{x} = -\widetilde{M}^*\ddot{\vec{x}}_{gN} + \vec{F}(t) + \vec{F}_A^{\,*}, \\
\widetilde{M}^* = diag\left[\widetilde{M}^*_1 \ldots \widetilde{M}^*_i \ldots \widetilde{M}^*_N\right] = 3N \times 3N, \\
\vec{F}_A^{\,*T} = \left[0, \ldots, F^*_{Aiy}, F^*_{Aiz}, M^*_{xi}/r_{Si} \ldots, 0\right], \\
F^*_{Aiy} = m^*_A\left[\ddot{v}_g + \ddot{v}_i - \left(z_{Ai} - z_{C_{Mi}}\right)\ddot{\theta}_i\right] + m^*_A\ddot{u}^*cos\gamma, \\
F^*_{Aiz} = m^*_A\left[\ddot{w}_g + \ddot{w}_i - \left(y_{Ai} - y_{C_{Mi}}\right)\ddot{\theta}_i\right] + m^*_A\ddot{u}^*sin\gamma,\ M^*_{Aix} \approx 0,
\end{gathered} \tag{12}$$

The approximated linearized equation of motion for TMD for the story number i is,

$$\begin{gathered}
\ddot{u}^* + 2\xi^*_A\omega^*_A\dot{u}^* + \omega^2_A u^* = \\
-\left[\ddot{v}_g + \ddot{v}_i - \left(z_{Ai} - z_{C_{Mi}}\right)\ddot{\theta}_i\right]cos\gamma - \left[\ddot{w}_g + \ddot{w}_i - \left(y_{Ai} - y_{C_{Mi}}\right)\ddot{\theta}_i\right]sin\gamma,
\end{gathered} \tag{13}$$

where $m_f(1 - k\underline{k})$ must be regarded as the dead fluid mass, thus slightly reducing the natural frequency of the main structure.

5. Method

This study aims to find the optimum design for the passive hybrid control system to reduce displacements and protect the base isolators by implementing isolators and TLCD devices on the base level of the structure. In this study, metaheuristic methods are used to establish the optimum design variables of base-isolators (stiffness and damping) and TLCD (shape properties to tune stiffness and damping). In this context, a benchmark model of a twenty-story base-isolated building is used. Details of the building are explained in a subsequent section.

Within the scope of this study, dynamic analysis of the benchmark base-isolated TLCD-controlled structure was conducted by generating motion equations of the structure and the hybrid systems. These equations were then modeled utilizing MATLAB with Simulink. Then, an optimization code was generated for optimizing the BI subsystem and TLCD system specifically for base-isolated structures. The JAYA metaheuristic algorithm was used in the optimization process. The effectiveness of the optimized hybrid control system was investigated by performing numerical simulations and comparing the results with the simple base-isolated structure without TLCD. Finally, the performance of the base-isolated TLCD-controlled structure was evaluated by applying different recorded ground motions as base excitations.

5.1. Benchmark Structure

A 20-story shear-beam-type building (n = 20) is considered in this investigation in which every story unit is identically constructed. The same benchmark structure was used previously in [34]. The structural properties of each story unit are as follows: m_i = mass of each floor = 300 tons; k_i = elastic stiffness of each floor = 10^6 KN/m; and C_i = internal damping coefficient of each floor = 2261 KN.s/m (corresponding to a damping ratio of the first mode ζ_1 = 0.005), and the height of each story h_i = 3 m. The computed natural frequencies for the building are 4.4, 13.2, 22, 30.6, 39, 47.2, up to 112.4, 114.1, and 115.1 rad/s.

5.2. Modal Tuning of TLCD

When the modes of the structure are well-determined, the two degrees of the freedom modally isolated coupled TLCD-frame system are still an approximation since the fluid mass of the TLCD impacting the main system is not taken into consideration in the dynamics of the main system. Metaheuristic algorithms could carry out the TLCD's modal tuning through analogy between equivalent TMD and TLCD.

5.2.1. Analogy between TMD and TLCD When Attached to the Symmetric Structure

Defining the relationship between u and u^* is the first step. The right side of the second equations in Equations (1) and (10), when compared, reveal that the same excitation is proportional.

$$u^* = u/k_j, \tag{14}$$

$$\omega^*{}_{Aj} = \omega_{Aj},\ \xi^*{}_{Aj} = \xi_{Aj} \tag{15}$$

$$\begin{gathered}
\frac{\mu_j \underline{k_j}}{1+\mu_j} = \frac{\mu^*{}_j}{k_j(1+\mu^*{}_j)}, \\
\frac{1}{1+\mu_j}\omega^2{}_{Sj} = \frac{1}{1+\mu^*{}_j}\omega^{*2}{}_{Sj}, \\
\frac{1}{1+\mu_j}2\xi_{Sj}\omega_{Sj} = \frac{1}{1+\mu^*{}_j}2\xi^*{}_{Sj}\omega^*{}_{Sj}, \\
\frac{1}{\varphi_j{}^T\widetilde{M}\varphi_j(1+\mu_j)} = \frac{1}{\varphi_j{}^T\widetilde{M}^*\varphi_j(1+\mu^*{}_j)},
\end{gathered} \tag{16}$$

and as a result, the analogous TMD-main system's mass ratio changes into,

$$\begin{gathered}
\mu^*{}_j = \frac{\mu_j k_j \underline{k_j}}{1+\mu_j(1-k_j\underline{k_j})} < \mu_j, \\
\delta_{jopt} = \frac{\omega_{Ajopt}}{\omega_{Sj}} = \frac{\delta_{jopt}{}^*}{\sqrt{1+\mu_j\left(1-k_j\underline{k_j}\right)}}, \\
\omega^*{}_{Sj} = \frac{\omega_{Sj}}{\sqrt{1+\mu_j\left(1-k_j\underline{k_j}\right)}} < \omega_{Sj}, \\
\xi^*{}_{Sj} = \frac{\xi_{Sj}}{\sqrt{1+\mu_j\left(1-k_j\underline{k_j}\right)}} < \xi_{Sj}
\end{gathered} \tag{17}$$

and,

$$m^*{}_j = m_j\Big(1 + \mu_j\Big(1 - k_j\underline{k_j}\Big)\Big) > m_j,$$
$$m_{Aj} = k_j\underline{k_j}m_{fj} < m_{fj}, \tag{18}$$

The conjugate main structural mass includes the dead fluid mass of the TLCD, $m_f\big(1 - k\underline{k}\big)$, $k\underline{k}$ i.e., should be maximal.

5.2.2. Analogy between TMD and TLCD When Attached to the Asymmetric Structure

The fundamental framework for utilizing the results of the TMD design is the analogy between TMD and TLCD attached to a multi-degree-of-freedom symmetric structure. Later, the method for a larger class of plan-asymmetric space structures with TLCD attached was researched, and the findings are helpfully summarized here. The modal mass ratio of the TMD-main system is defined by,

$$\mu^*{}_j = \mu_j \frac{k_j\underline{k_j}(V^*{}_j/V_j)^2}{1 + \mu_j(1 - k_j\underline{k_j}(V^*{}_j/V_j)^2)} < \mu_j, \tag{19}$$

The frequency and damping ratio of the modified main system with an equivalent TMD are defined by,

$$\omega^*{}_{Sj} = \frac{\omega_{Sj}}{\sqrt{1 + \mu_j(1 - k_j\underline{k_j}(V^*{}_j/V_j)^2)}} < \omega_{Sj},$$
$$\xi^*{}_{Sj} = \frac{\xi_{Sj}}{\sqrt{1 + \mu_j\Big(1 - k_j\underline{k_j}(V^*{}_j/V_j)^2\Big)}} < \xi_{Sj}, \tag{20}$$

The TMD frequency ratio $\delta^*{}_{jopt} = \frac{\omega^*{}_{Ajopt}}{\omega^*{}_{Sj}}$ and the TLCD frequency ratio $\delta_{jopt} = \frac{\omega_{Ajopt}}{\omega_{Sj}}$ are thus related by the more general transformation,

$$\delta_{jopt} = \frac{\delta^*{}_{jopt}}{\sqrt{1 + \mu_j\Big(1 - k_j\underline{k_j}(V^*{}_{ij}/V_{ij})^2\Big)}} < \delta^*{}_{jopt}, \tag{21}$$

This results in a slightly lower ideal frequency ratio δ_{jopt} for the TLCD than for an equivalent TMD. The ideal damping coefficient does not vary $\xi_{Ajopt} = \xi^*{}_{Ajopt}$. The dead fluid mass that appears in the denominator of Equations (25) through (27) alters the primary system, written as,

$$1 + \mu_j\left(1 - k_j\underline{k_j}\left(\frac{V^*{}_{ij}}{V_{ij}}\right)^2\right) = m_{fj}\Big(1 - (k_jV^*{}_{ij}/V_{ij})^2\Big),$$
$$for\ k_j = \underline{k_j}\ and\ m_j = 1, \tag{22}$$

The higher value of the geometry factor *j* must be attained while remaining inside the boundaries of the liquid column in order to minimize the former. Hmax $|u| \leq 2/3$H.

5.3. The Metaheuristic Algorithm-Based Optimization

This section describes the structural control system's metaheuristic algorithm-based optimization approach. The general methodology of the optimization process is based on generating candidate solutions and identifying the best solution by altering current candidate solutions in accordance with the optimization's goal.

5.3.1. Steps of Optimization Process

In light of how this process functions, optimization can be summed up in the following 5 steps:

Step 1: The population number (pn), the user-specified algorithmic parameters, the design constants, the lower and upper bounds of the design variable, and the stopping criteria of the optimization problem are all defined. The maximum iteration number defines the stopping criteria in this chapter.

Step 2: As demonstrated in Equation (23), a value is generated at random for each design variable that falls within its lower and upper bounds. Up until the population number specified in Step 1 is given, this process is repeated.

$$X_{i,j} = X_{i(low)} + rand \cdot (X_{i(up)} - X_{i(low)}), \tag{23}$$

The numbers i and j in Equation (24) stand for the number of design variables and solution vectors, respectively. $X_{i,j}$, $X_{i(low)}$, and $X_{i(up)}$ show the value of the design variable and the lower and upper limit of the design variable, respectively. With the Rand command, we can produce random numbers between 0 and 1. Following that, these generated values are kept in an initial solution matrix such as the CL matrix in Equation (24),

$$\begin{gathered}\mathrm{CL} = [X_{1,1}\ X_{1,2}\ \cdots\ X_{1,pn}\ X_{2,1}\ X_{2,2}\ \cdots\ X_{2,pn} \vdots \vdots \cdots \vdots \\ X_{N-1,1}\ X_{N-1,2}\ \cdots\ X_{N-1,pn}\ X_{N,1}\ X_{N,2}\ \cdots\ X_{N,pn}],\end{gathered} \tag{24}$$

Every column of the CL matrix is a potential solution vector that contains values for the design variables. There are pn solution vectors and N design variables in the matrix.

Step 3: The optimization problem's design constraints (limitation of control system movements) are examined, and the objective function is calculated for each solution vector. The objective function of the associated solution is provided as a penalized value if a solution vector does not provide a design constraint. The reduction of structural response is the objective function. Many cases will be considered in the study since displacement and acceleration may show different behavior for base-isolated structures.

Step 4: New solutions are generated and stored in a new solution matrix in this step. This stage is particular to the type of algorithm since the generation is carried out in accordance with the algorithm principles.

In this research, the JAYA [35] metaheuristic algorithm was tested and modified to find the best performance. The algorithm is presented shortly in this section.

In the optimization process performed with the JAYA algorithm, new solutions are created by using the already existing design variables in the initial solution matrix by applying the JAYA algorithm equation, Equation (25). Details of this equation are presented in Table 1. JAYA is a single-phase metaheuristic algorithm, and it makes the application of this method easy.

$$X_{i,new} = X_{i,j} + rand()\left(X_{i,g\ best} - |X_{i,j}|\right) - rand()(X_{i,g\ worst} - \left|X_{i,j}\right|), \tag{25}$$

Table 1. JAYA optimization components.

	Variable	Description
Optimization Components	$X_{i,new}$	New value for the design variable i
	$X_{i,j}$	The design variable value for the candidate solution j in the initial matrix
	$X_{i,g\ best}$	The best solution value for the design variable i in terms of objective function
	$X_{i,g\ worst}$	The worst solution value for the design variable i in terms of objective function

Step 5: The final step compares the new solution matrix to the current (old) solution matrix. The old solution matrix is updated if the new solutions' goal functions outperform the current ones.

Up until the maximum iteration number, which is the stopping criteria, is given, Steps 4 and 5 are repeated.

In this article, the code will be generated with MATLAB, and the dynamic analysis with structural control will be integrated via MATLAB SIMULINK.

5.3.2. Limitations

The upper and lower limitations of the parameters of BI subsystem and TLCD system that were defined as constraints in the optimization process for this study are shown in Table 2. Where B is the liquid columns' horizontal length, Beta is the angle between the inclined pipes and X direction, Cr is the damping ratio of TLCD; H is the liquid columns' inclined length; AH is the inclined liquid columns' cross-sectional area; AB is the horizontal liquid columns' cross-sectional area; Alpha = m_h/m_{TLCD}: m_h is the mass of liquid in the horizontal pipe and m_{TLCD} is the mass of TLCD; Gamma = 1 − TLCD Mass Ratio + (TLCD Mass Ratio/Alpha^2), K1 and K2 are geometry factors of TLCD; U is the liquid's relative displacement; Cb is the damping ratio of BI; Tb is the period of BI; and Xb is the displacement of the base.

Table 2. Constraints of BI and TLCD's parameters.

Controller Type	Parameters	Units	Constraints	
			Minimum	Maximum
TLCD	B	m	0.01	10
	Beta	radian	$\pi/4$	$\pi/2$
	Cr	%	1	50
	H	m	0.01	10
	AH	m^2	0.01	50
	AB	m^2	0.01	50
	TLCD Mass Ratio	%	-	5
	Alpha	-	0	1
	Gamma	-	1	-
	K1	-	-	1
	K2	-	-	1
	U	m	-	H
Base Isolation	Cb	%	0.01	40
				30
				20
				15
				10
	Tb	s	1	5
	Xb	m	-	40
			-	35
			-	30

6. Results

The control performances of the structure are examined for three scenarios using time history analyses with selected recorded ground excitations: the simple structure without control, the base-isolated structure, and the base-isolated structure with an attached TLCD device. Results are based on 44 far-field ground motions (2 horizontal records in each station) that were recorded from severe seismic events with moment magnitudes between 6.5 and 7.6 that were recorded on NEHRP site classes C (soft rock) and D (stiff soil). These motions are part of the FEMA P-695-FF set described in [36]. The details of the records of the FEMA P-695 far-field set are given in Table 3.

With the benchmark structure and the previously mentioned 44 earthquake excitations, time histories of all response quantities were computed. Within 60 s of the earthquake episodes, maximum displacement, maximum total acceleration, and maximum interstory drift of the roof level under 4 earthquake effects as examples are shown in Table 4. Under such strong earthquakes, all response quantities of the unprotected building are excessive.

To reduce the structural response, a rubber-bearing isolation subsystem was implemented, Figure 2a. The mass of the base-isolation subsystem is m_b = 300 tons. The response of a base-isolation subsystem is assumed as linear. The damping ratio and period of the base-isolation subsystem were optimized by using the JAYA algorithm with three different cases. One case entailed a 40 cm maximum displacement and 40% maximum damping ratio of base-isolation subsystem, another case had 40 cm maximum displacement and 20% maximum damping ratio, and the last case had 35 cm maximum displacement and 20% maximum damping ratio. The optimized properties of the base-isolation subsystem are shown in Table 5.

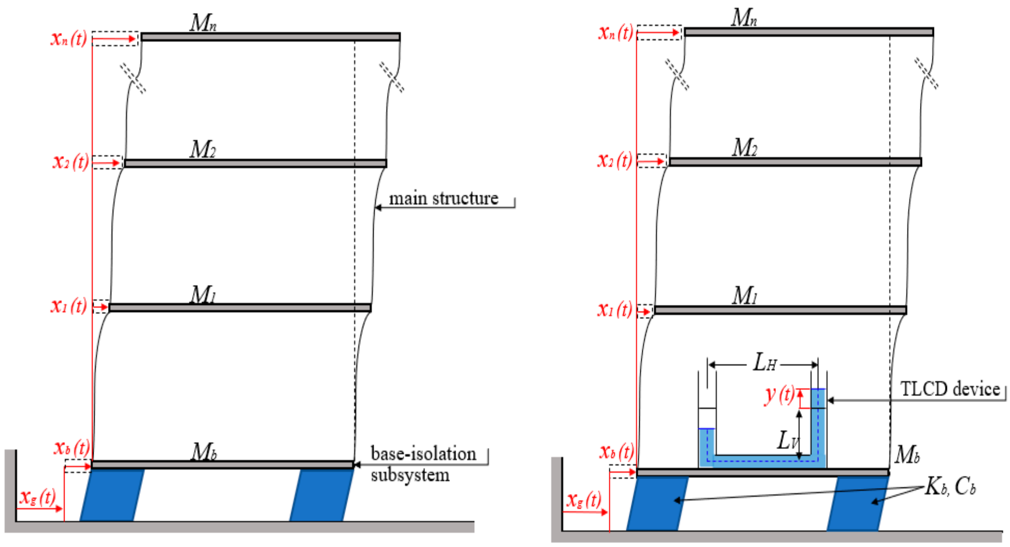

Figure 2. Base-isolated MDOF shear-type frame structures: (**a**) without TLCD; (**b**) with TLCD.

Table 3. FEMA P-695 far-field ground motion records.

Earthquake No.	Earthquake			Site Data		Source (Fault Type)	Site-Source Distance (km)		Lowest Freq (Hz.)	Recorded Motions	
	Magnitude	Year	Name	NEHRP Class	Vs_30 (m/s)		Epicentral	Closest to Plane		PGA Max (g)	PGV Max (cm/s.)
1–2	6.7	1994	Northridge	D	356	Thrust	13.3	17.2	0.25	0.52	63
3–4	6.7	1994	Northridge	D	309	Thrust	26.5	12.4	0.13	0.48	45
5–6	7.1	1999	Duzce, Turkey	D	326	Strike-slip	41.3	12	0.06	0.82	62
7–8	7.1	1999	Hector Mine	C	685	Strike-slip	26.5	11.7	0.04	0.34	42
9–10	6.5	1979	Imperial Valley	D	275	Strike-slip	33.7	22	0.06	0.35	33
1–12	6.5	1979	Imperial Valley	D	196	Strike-slip	29.4	12.5	0.25	0.38	42
13–14	6.9	1995	Kobe, Japan	C	609	Strike-slip	8.7	7.1	0.13	0.51	37
15–16	6.9	1995	Kobe, Japan	D	256	Strike-slip	46	19.2	0.13	0.24	38
17–18	7.5	1999	Kocaeli, Turkey	D	276	Strike-slip	98.2	15.4	0.24	0.36	59
19–20	7.5	1999	Kocaeli, Turkey	C	523	Strike-slip	53.7	13.5	0.09	0.22	40
21–22	7.3	1992	Landers	D	354	Strike-slip	86	23.6	0.07	0.24	52
23–24	7.3	1992	Landers	D	271	Strike-slip	82.1	19.7	0.13	0.42	42
25–26	6.9	1989	Loma Prieta	D	289	Strike-slip	9.8	15.2	0.13	0.53	35
27–28	6.9	1989	Loma Prieta	D	289	Strike-slip	31.4	12.8	0.13	0.56	45
29–30	7.4	1990	Manjil, Iran	C	724	Strike-slip	40.4	12.6	0.13	0.51	54
31–32	6.5	1987	Superstition Hills	D	192	Strike-slip	35.8	18.2	0.13	0.36	46
33–34	6.5	1987	Superstition Hills	D	208	Strike-slip	11.2	11.2	0.25	0.45	36
35–36	7	1992	Cape Mendocino	D	312	Thrust	22.7	14.3	0.07	0.55	44
37–38	7.6	1999	Chi-Chi, Taiwan	D	259	Thrust	32	10	0.05	0.44	115
39–40	7.6	1999	Chi-Chi, Taiwan	C	705	Thrust	77.5	26	0.05	0.51	39
41–42	6.6	1971	San Fernando	D	316	Thrust	39.5	22.8	0.25	0.21	19
43–44	6.5	1976	Friuli, Italy	C	425	Thrust	20.2	15.8	0.13	0.35	31

Table 4. Examples for the structural responses of base and roof levels.

	Maximum Limitation of Base Isolation's Displacement		**40 cm**				**35 cm**			
	Maximum Limitation of Base Isolation's Damping Ratio		**40%**		**20%**		**20%**			
	Earthquake No.		**21**		**9**		**37**		**38**	
	Structural Response	**Units**	**Base**	**Roof**	**Base**	**Roof**	**Base**	**Roof**	**Base**	**Roof**
Displacement	no control	m	-	0.573	-	0.233	-	0.493	-	0.298
	with BI	m	0.11549	0.1673	0.15	0.228	0.257	0.42	0.357	0.592
	with BI & TLCD	m	0.11547	0.1672	0.149	0.226	0.247	0.4	0.35	0.586
	Reduction Value with Hybrid Control	m	2×10^{-5}	0.406	0.001	0.007	0.01	0.093	0.007	−0.288
	Reduction Ratio	%	0.02	70.8	1.3	3	3.9	18.9	2	−96.6
Total Acceleration	no control	m/s^2	-	12.4	-	7	-	10.4	-	8.6
	with BI	m/s^2	1.09	1.49	1.3	1.47	2.63	3	2.9	4.37
	with BI & TLCD	m/s^2	1.10	1.50	1.28	1.49	2.56	2.9	3	4.38
	Reduction Value with Hybrid Control	m/s^2	−0.01	11	0.02	5.5	0.07	7.5	−0.03	4.2
	Reduction Ratio	%	−0.9	88	1.5	78.7	2.7	72.1	−1	49.2
Interstory Drift	no control	m	-	0.0037	-	0.0021	-	0.0031	-	0.0026
	with BI	m	0.0053	448×10^{-6}	673×10^{-5}	44×10^{-5}	0.0149	0.0009	0.021	1312×10^{-6}
	with BI & TLCD	m	0.0054	45×10^{-5}	672×10^{-5}	45×10^{-5}	146×10^{-4}	88×10^{-5}	0.0212	1313×10^{-6}
	Reduction Value with Hybrid Control	m	−0.0001	0.0033	2×10^{-6}	0.0016	3×10^{-4}	0.0022	-2×10^{-4}	0.0013
	Reduction Ratio	%	−1.9	88	0.03	78.7	2	71.8	−1.1	49.2

With such an optimized base-isolation subsystem, the fundamental natural frequencies of the three optimized cases became w_1 = 2.28, w_2 = 2.31, and w_3 = 2.58 rad/s.

Within 60 s of the earthquake episodes, the maximum displacement, maximum total acceleration, and maximum interstory drift of the roof and base levels under the same 4 earthquakes are shown in Table 4.

To protect the safety and integrity of the base-isolation subsystem, a passive TLCD was connected to it as shown in Figure 2b, referred to as the passive hybrid control system. The properties of this TLCD were optimized by using the JAYA algorithm specifically for the investigated base-isolated building in order to guarantee the best response of the structure under earthquake effects. The optimized TLCD properties for three different cases are shown in Table 6.

Table 5. Properties of optimized base-isolated subsystem.

Case No.			1	2	3
Maximum Limitation of Base Isolation's Displacement			**40 cm**		**35 cm**
Maximum Limitation of Base Isolation's Damping Ratio			**40%**	**20%**	**20%**
Controller Type	**Parameters**	**Units**	**Optimum Values**		
Base Isolation	Damping Ratio Cb	%	20.85	19.29	19.82
	Period Tb	s	2.42	2.38	2.06
	Elastic Stiffness Kb	KN/m	42,596	44,619	61,342
	Damping Coefficient Cb	KN·s/m	68,414	652,050	797,220

Table 6. Properties of optimized TLCD system.

Case No.			1	2	3
Maximum Limitation of Base Isolation's Displacement			**40 cm**		**35 cm**
Maximum Limitation of Base Isolation's Damping Ratio			**40%**	**20%**	**20%**
Controller Type	**Parameters**	**Units**	**Optimum Values**		
TLCD	B	m	10	10	6.297
	Beta	radian	1.31	0.84	0.89
	Cr	%	14.6	2.2	35.9
	H	m	10	10	7.88
	AH	m^2	0.94	3.62	11.54
	AB	m^2	0.01	2.96	17.76
	WTLCD	red/s	0.14	0.67	0.88
	TTLCD	s	44.7	9.32	7.18
	Mass Ratio (TLCD)	%	0.32	1.7	4.9
	Alpha	-	0.005	0.29	0.381
	Gamma	-	113.4	1.18	1.29
	K1	-	0.016	0.72	0.82
	K2	-	0.76	0.83	0.64

With such a passive hybrid control system, the maximum displacement, maximum total acceleration, and maximum interstory drift of the base and top levels within 60 s of the same 4 earthquake episodes are presented in Table 4.

The displacement, total acceleration, and interstory drift of the base-isolation subsystem as well as all story beams were estimated for the simple uncontrolled structure, base-isolated structure, and TLCD-controlled base-isolated structure for each of the FEMA P-695-FF 44 records. In this regard, Figures 3 and 4 show a comparison of the profile of peak response quantities of the simple uncontrolled structure (red line), the base-isolated structure with (green line) and without (blue line) TLCD under earthquakes no. 37 and 21, respectively. Further, the maximum structural responses of the base and roof levels for the hybrid-controlled structure are summarized in Table 7.

Two records of the considered FEMA P-695-FF record set, specifically earthquakes no. 21 and 37, are portrayed in Figure 5, while a comparison among the corresponding response time histories of the simple uncontrolled structure and the base-isolated benchmark structure with and without TLCD are shown in Figures 6 and 7 for the roof and base levels under earthquake no. 37 and in Figures 8 and 9 for the roof and base levels under earthquake no. 21, respectively.

Table 7. The maximum structural responses of the base and roof levels under 44 earthquakes: effects for the hybrid controlled structure.

Maximum Limitation of Base Isolation's Displacement			**40 cm**				**35 cm**	
Maximum Limitation of Base Isolation's Damping Ratio			**40%**		**20%**		**20%**	
Structural Response		**Units**	**Base**	**Roof**	**Base**	**Roof**	**Base**	**Roof**
Displacement	Maximum	m	0.4	0.587	0.4	0.595	0.35	0.586
	Maximum Reduction by Using TLCD	m	0.0002	0.0001	0.0048	0.0043	0.01	0.019
	Reduction Ratio	%	0.07	0.04	1.3	0.8	3.9	4.6
	Effectiveness Ratio	%	54.6	31.8	88.6	54.5	88.6	68.2
Acceleration	Maximum	m/s^2	2.9	3.9	2.9	3.9	3.15	4.63
	Maximum Reduction by Using TLCD	m/s^2	0.015	0.02	0.027	0.025	0.13	0.17
	Reduction Ratio	%	0.9	0.6	1.9	0.7	7.8	5.1
	Effectiveness Ratio	%	45.45	34.1	27.3	22.7	36.4	22.7
Interstory Drift	Maximum	m	0.017	0.0012	0.018	0.0012	0.0212	0.0014
	Maximum Reduction by Using TLCD	m	4×10^{-6}	7×10^{-6}	2×10^{-5}	7×10^{-6}	3×10^{-4}	5×10^{-5}
	Reduction Ratio	%	0.07	0.0007	0.14	0.7	2	5.2
	Effectiveness Ratio	%	13.6	34.1	11.4	20.4	18.2	22.7

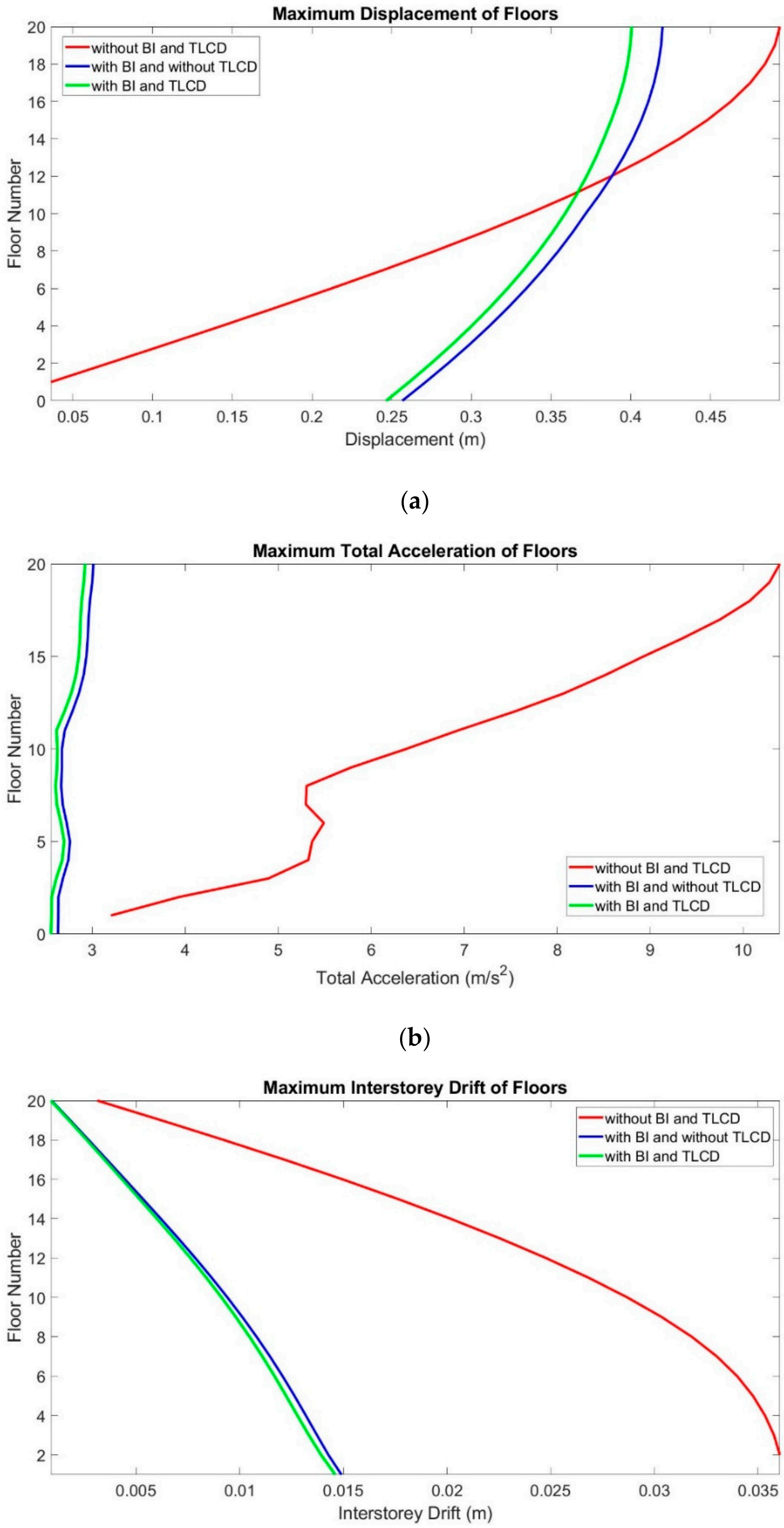

(**a**)

(**b**)

(**c**)

Figure 3. Peak response profiles for hybrid-controlled structure, base-isolated structure, and simple uncontrolled structure subjected to earthquake no. 37 record: (**a**) maximum displacement; (**b**) maximum total acceleration; (**c**) maximum interstory drift.

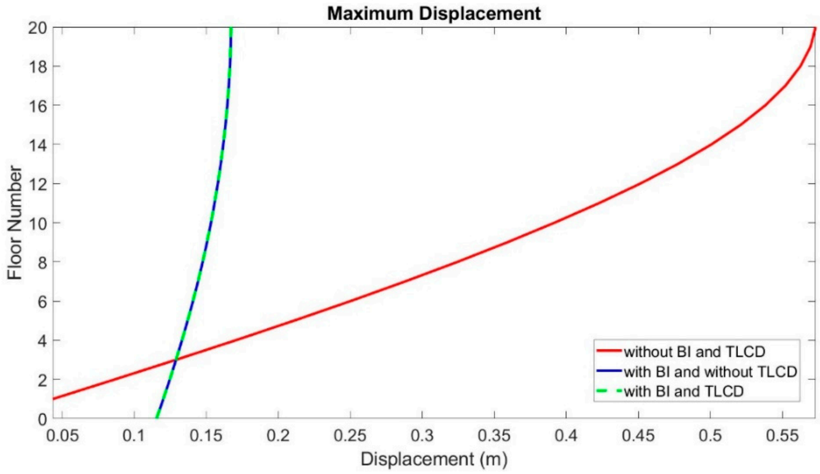

(**a**)

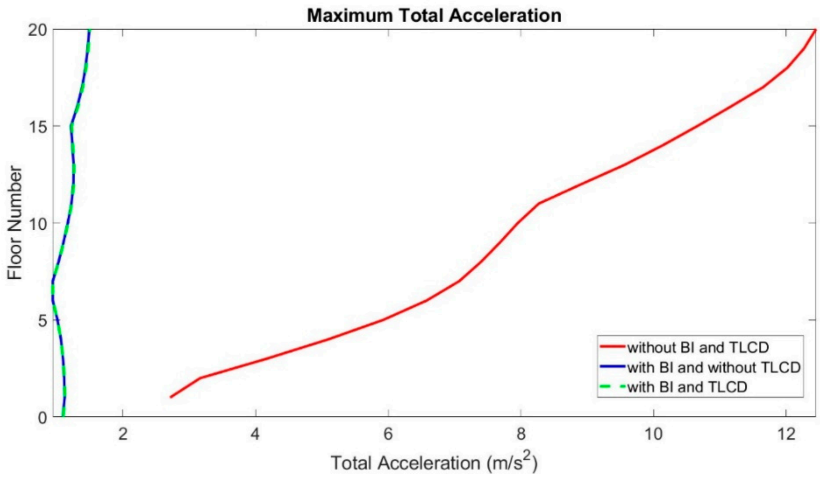

(**b**)

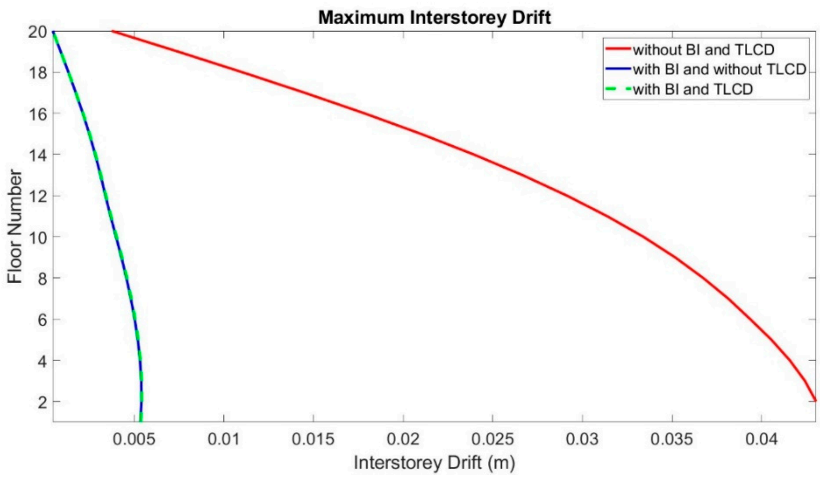

(**c**)

Figure 4. Peak responses for a hybrid-controlled structure, base-isolated structure, and simple uncontrolled structure subjected to earthquake no. 21 record: (**a**) maximum displacement; (**b**) maximum total acceleration; (**c**) maximum interstory drift.

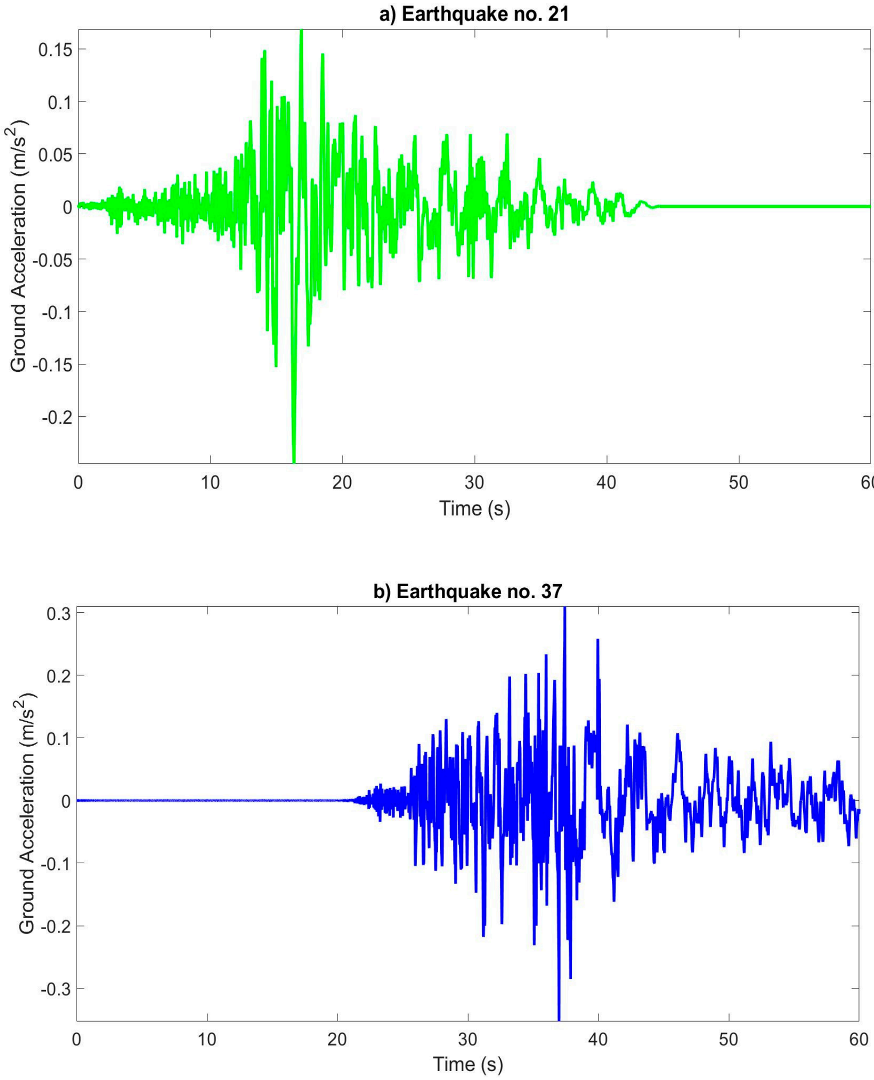

Figure 5. Two accelerograms of the FEMA P-695-FF record set: (**a**) earthquake no. 21; (**b**) earthquake no. 37.

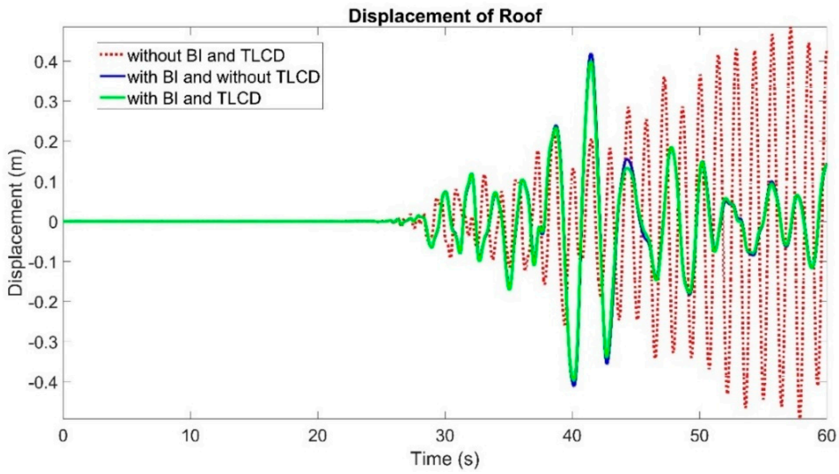

(**a**)

Figure 6. *Cont.*

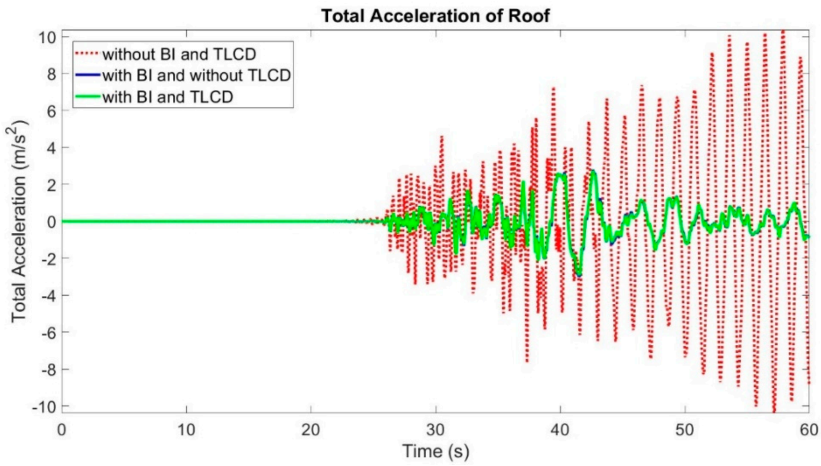

(**b**)

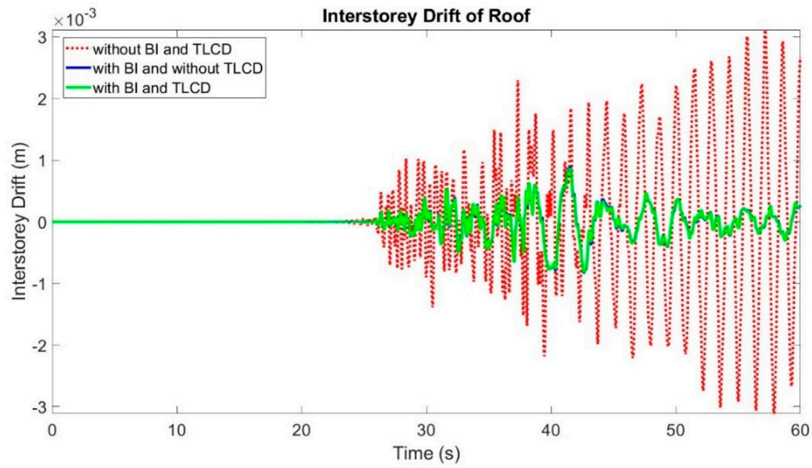

(**c**)

Figure 6. Response time histories of the roof level for the earthquake-prone simple uncontrolled structure, base-isolated structure, and hybrid-controlled structure no. 37 record: (**a**) displacement; (**b**) total acceleration; (**c**) interstory drift.

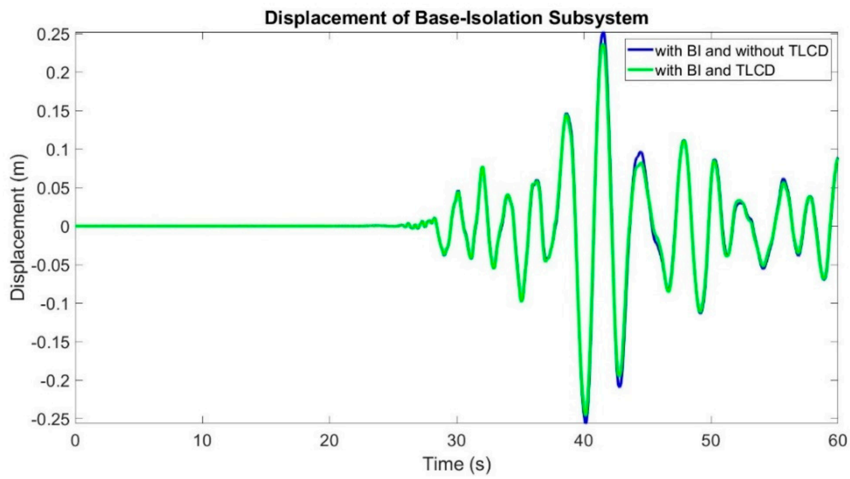

(**a**)

Figure 7. *Cont.*

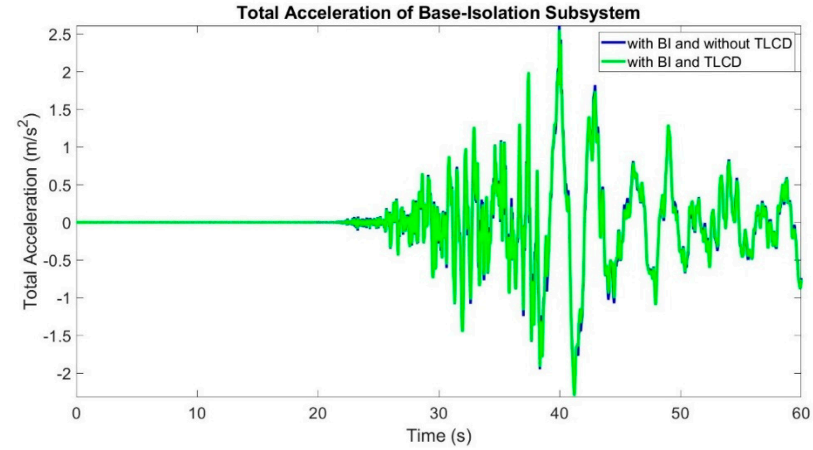

(**b**)

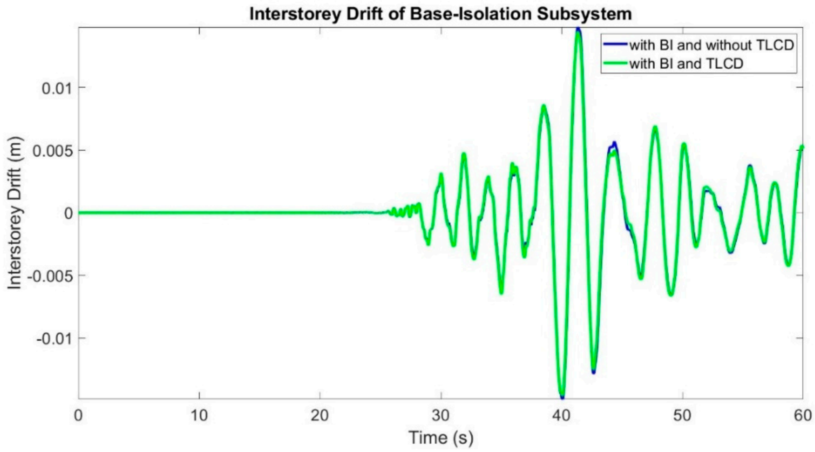

(**c**)

Figure 7. Response time histories of the base level for the earthquake-prone simple uncontrolled structure, base-isolated structure, and hybrid-controlled structure no. 37 record: (**a**) displacement; (**b**) total acceleration; (**c**) interstory drift.

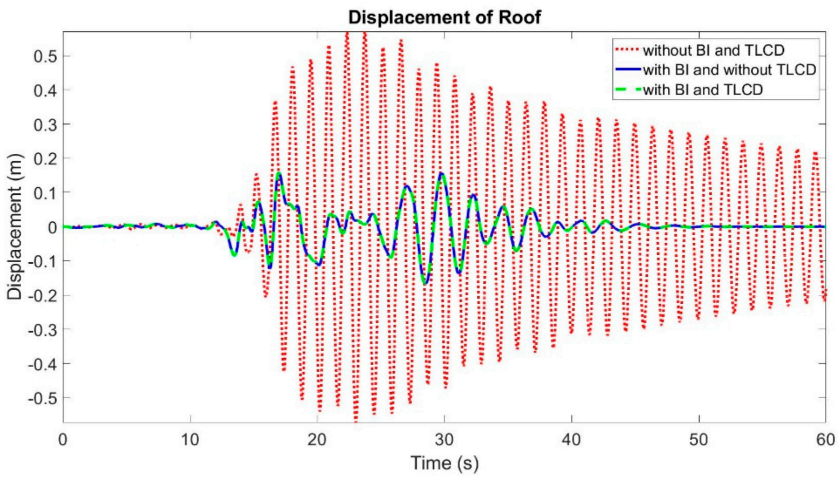

(**a**)

Figure 8. *Cont*.

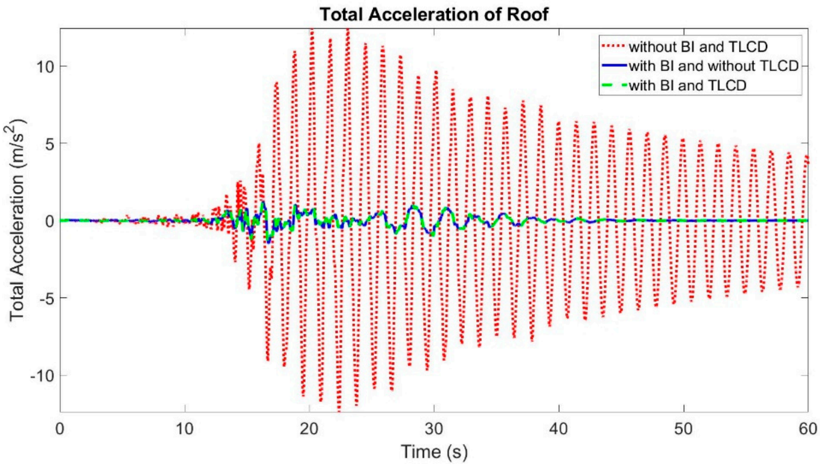

(**b**)

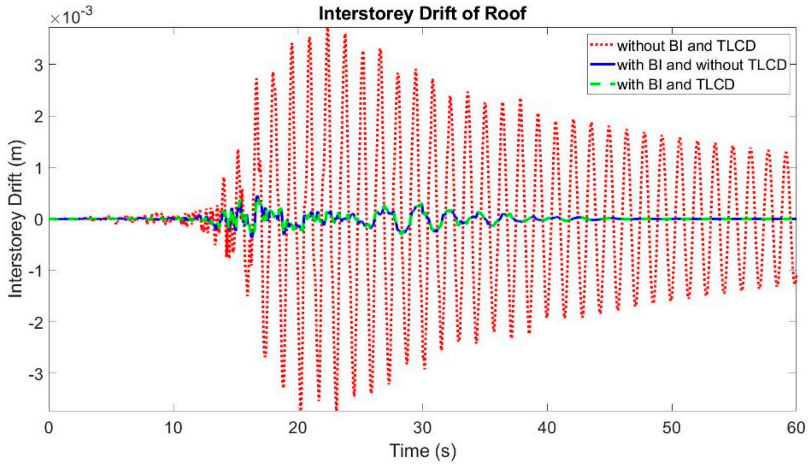

(**c**)

Figure 8. Response time histories of roof level for the earthquake-prone simple uncontrolled structure, base-isolated structure, and hybrid-controlled structure no. 21 record: (**a**) displacement; (**b**) total acceleration; (**c**) interstory drift.

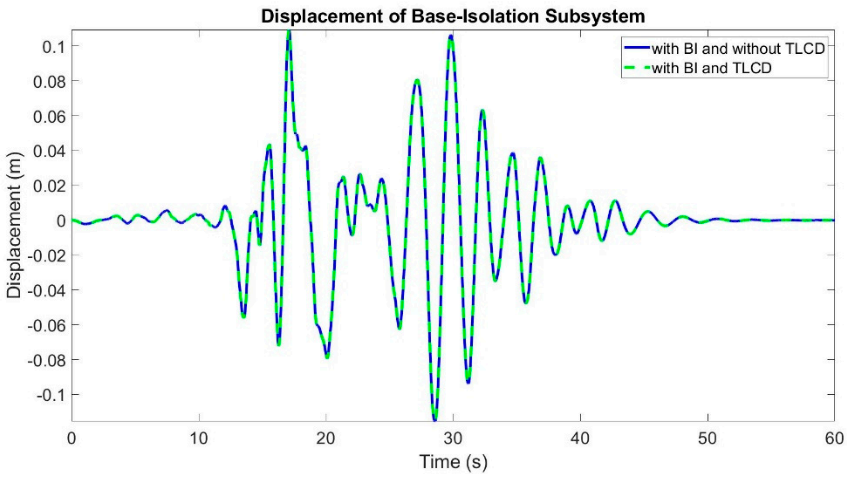

(**a**)

Figure 9. *Cont.*

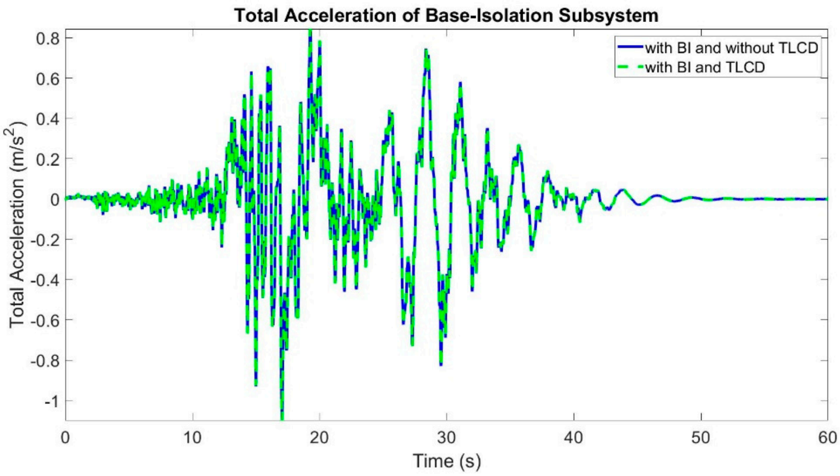

(**b**)

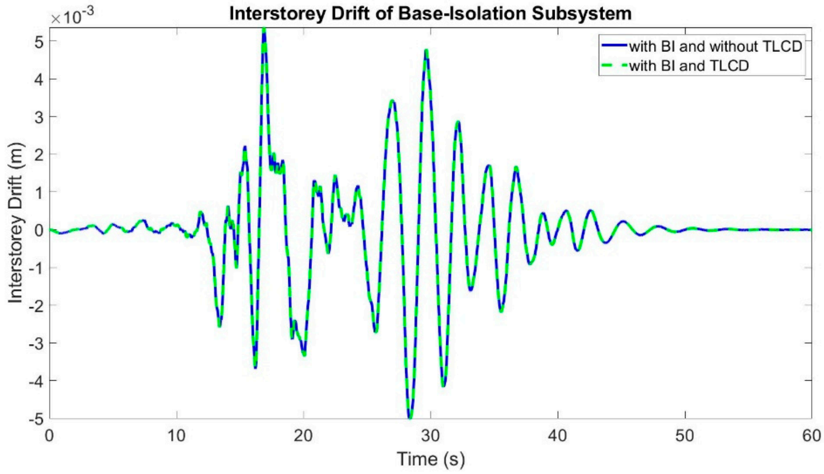

(**c**)

Figure 9. Response time histories of base level for the earthquake-prone simple uncontrolled structure, base-isolated structure, and hybrid-controlled structure no. 21 record: (**a**) displacement; (**b**) total acceleration; (**c**) interstory drift.

7. Discussion

Through a base-isolation subsystem, the structure is virtually decoupled from the ground by shifting the fundamental natural frequency of the entire structural system away from the range of frequencies that dominate the earthquake excitation [7]. The fundamental natural frequency of the structure is reduced by the implementation of a base-isolation (BI) subsystem; it is reduced in this work by 48.4%, 47.7%, and 41.6% by using the three cases of the optimized base-isolation subsystem. Table 4 shows that the interstory drifts and total accelerations of the roof floor are reduced for all cases. Although the displacements of the roof floor are reduced for most cases, using BI might cause a negative effect, such as in the case of earthquake number 38, where the displacement of the roof was increased. Based on the results in Table 4, the advantage of using a base-isolation subsystem to protect the building is considered demonstrated. On the other hand, the responses of the base-isolation subsystem are usually massive [37]. However, in our case, the BI subsystem's properties were optimized specifically for the investigated building which kept the displacements of BI below the maximum limitations. Nevertheless, displacements of BI might exceed the maximum limit in some cases, such as in the case of earthquake number 38, where BI alone could not keep the maximum displacement below 35 cm as shown in Table 4.

In addition, Table 4 shows that the interstory drifts and total accelerations of the base and top levels have no noticeable change when connecting a passive TLCD to the base-isolation subsystem. However, displacements of the base and roof were reduced in all cases, but this reduction in some cases is very minor, not worthy to be mentioned. In other cases, the reduction value is noticeable but very small. For example, the reduction ratio of base displacements is between 0.02% and 3.9%. On the other hand, this small reduction has a very big effect in reducing BI subsystem displacements and keeping them below the maximum limit when the BI subsystem alone is not enough to control the structural response and keep it within the limits. This is the same as the case of earthquake number 38 where the displacement of the BI Subsystem without TLCD was 35.7 cm which exceeded the maximum limit of 35 cm. By using a TLCD system attached to the BI subsystem, the displacement was reduced to be equal to the maximum limit, and thus the safety and integrity of the BI subsystem were protected.

The designs of the base-isolation subsystem and TLCD device were specifically optimized by using the JAYA algorithm for the 20-story investigated structure. Moreover, both of the systems were optimized considering using the other system in the structure. During the optimization process, two limitations were taken into consideration: the maximum displacement and maximum damping ratio of the base-isolation subsystem (Tables 5 and 6). The first case of optimization was with a maximum BI's displacement of 40 cm and a maximum BI's damping ratio of 40%. The second case was with the same maximum displacement and 20% maximum damping ratio. The third case was for 35 cm maximum displacement and 20% maximum damping ratio.

As apparent in Figure 2, the optimized hybrid control system can effectively reduce the structural responses of the structure. The reduction at the roof reached a maximum of 70.8% in displacement demand and 88% in acceleration and interstory drift demands. The TLCD device when connected to the base-isolation subsystem could reduce the displacement demand of the base, with a maximum reduction of 3.9%. It is important to emphasize that this slight decrease in base displacement can preserve the safety of the base-isolation subsystem. On the other hand, the acceleration and interstory drift of the base were reduced in some cases and increased in other cases as shown in Table 4. However, the increase of acceleration and interstory drift of the base did not exceed 1.9%, and the reduction could reach a maximum of 2.7%.

The time histories of all the response values can also reveal similar results. However, it is evident from a careful examination of the responses to each of the 44 records that there may be circumstances in which the TLCD has only a minor impact on lowering the base-isolation system's displacement.

Figure 7 for earthquake record number 37 shows that the peak base-isolation displacement was significantly reduced by about 3.9% because of the TLCD device. Additionally, the peak roof displacement was decreased by nearly 18.9% (Figure 6). However, when taking into account the earthquake no. 21 record, a distinct tendency is apparent, as illustrated in Figures 8 and 9. In this instance, the TLCD device only reduced the peak base-isolation subsystem displacement by 0.02% (Figure 9). TMD-controlled structures [38] or TMD-controlled base-isolated structures [13,30] exhibit this behavior quite frequently. This is specifically because in the initial few seconds after excitation, passive control devices (such TLCDs and TMDs) have little impact on structural responses. Therefore, TLCDs cannot considerably lower maximum base-isolation subsystem displacement if the strongest reaction occurs early in the earthquake record, as in the case of earthquake number 21. Utilizing an active TLCD would be advised for such excitation [16]. Despite this, the base-isolation subsystem's safety and integrity seemed to be maintained while the displacement demand was reduced thanks to the passive control device. The proposed TLCD-controlled base-isolated system is simple enough for practical usage, considering the TLCD-positive features (low maintenance, easy installation, and mass of water is usable for firefighting), and considering that such a device would be positioned on the ground level when a reduction in the displacement demand of the base-isolation system is required.

As evident from Table 7, the maximum displacement of the base did not exceed the maximum limit in all cases. In addition, using a TLCD system for the base-isolated structure was effective in reducing the displacement of the base with a minimum ratio of 54.6% and a maximum ratio of 88.6% of the 44 earthquakes.

8. Conclusions and Recommendations

Conclusions reached based on the results obtained from the study are summarized as follows:

1. The fundamental natural frequency of the structure is reduced by the implementation of a base-isolation subsystem.
2. The interstory drifts and total accelerations of the roof floor are reduced by using a base-isolation subsystem.
3. Although the displacements of the roof floor are reduced for most cases, using BI might cause a negative effect in which displacements of the roof have a chance to increase.
4. The responses of the base-isolation subsystem are usually massive. However, in our case, the BI subsystem's properties were optimized specifically for the investigated building which kept the displacements of BI below or equal to the maximum limitations for most of the cases. Nevertheless, displacements of BI might exceed the maximum limit in some cases.
5. When a passive TLCD is connected to the base-isolation subsystem, there are no discernible changes to the interstory drifts and total accelerations of the base and top levels.
6. Base and roof displacements are lessened when a passive TLCD is connected to a base-isolation subsystem. However, this reduction in some cases is very minor, not worthy to be mentioned, and in other cases, the reduction value is noticeable but very small.
7. The small reduction in displacements of the base when connecting a passive TLCD to the base-isolation subsystem has a very big effect in keeping them below or equal to the maximum limit when the BI subsystem alone is not enough to control the structural response.
8. There may be instances where the TLCD has relatively little impact on lowering the base-isolation subsystem's displacement demand. This is specifically because in the initial few seconds after excitation, passive control devices (such TLCDs and TMDs) have little impact on structural responses. Therefore, TLCDs are unable to significantly lower the maximum base-isolation subsystem displacement if the highest response occurs early in the seismic record.
9. The maximum displacement of the base did not exceed the maximum limit in all cases where a TLCD was attached.
10. Using a TLCD system for the base-isolated structure was effective in reducing the displacement of the base with a minimum ratio of 54.6% and a maximum ratio of 88.6% in the 44 earthquakes.

Based on the results and conclusions above, the passive TLCD system appears to be quite effective in protecting and maintaining the safety and integrity of the base-isolation subsystem. In addition, the proposed passive hybrid control system can effectively reduce the structural responses of the structure. The significant advantage of such a passive hybrid control system is that the passive TLCD system is easy to design, install, and maintain, especially if the TLCD is on the ground level. The proposed TLCD-controlled base-isolated structure is simple enough for practical usage, considering the TLCD positive features (low maintenance, easy installation, and usability of mass of the water for firefighting) and that such a device would be positioned on the ground level when a reduction in the displacement demand of the base-isolation system is needed.

This research can be extended by considering the effect of locating an additional TLCD in the roof level in addition to the proposed hybrid control system in order to overcome the possible negative effect.

Author Contributions: Conceptualization, B.S., G.B. and S.M.N.; methodology, B.S., G.B., S.M.N. and A.E.K.; software, B.S., S.M.N. and A.E.K.; validation, B.S., G.B. and Y.E.I.; formal analysis, B.S.; investigation, B.S.; data curation, B.S. and S.M.N.; writing—original draft preparation, B.S., G.B., S.M.N. and A.E.K.; writing—review and editing, Y.E.I., M.N. and M.E.; visualization, B.S.; supervision, G.B. and Y.E.I.; project administration, Y.E.I., M.N. and M.E.; funding acquisition, Y.E.I., M.N. and M.E. All authors have read and agreed to the published version of the manuscript.

Funding: This research was funded by the Research and Initiatives Center, Prince Sultan University, Saudi Arabia in 2022.

Institutional Review Board Statement: Not applicable.

Informed Consent Statement: Not applicable.

Data Availability Statement: The data of the paper can be provided by conducting corresponding authors.

Acknowledgments: The authors thank Prince Sultan University for funding the research project and supporting the publication of this article.

Conflicts of Interest: The authors declare no conflict of interest.

References

1. Saifullah, M.K.; Alhan, C. Necessity and adequacy of near-source factors for seismically isolated buildings. *Earthq. Struct.* **2017**, *12*, 91–108. [CrossRef]
2. Chigira, M.; Wu, X.; Inokuchi, T.; Wang, G. Landslides induced by the 2008 Wenchuan earthquake, Sichuan, China. *Geomorphology* **2010**, *118*, 225–238. [CrossRef]
3. Margesson, R.; Taft-Morales, M. *Haiti Earthquake: Crisis and Response*; Library of Congress, Congressional Research Service: Washington, DC, USA, 2010.
4. Chimamphant, S.; Kasai, K. Comparative response and performance of base-isolated and fixed-base structures. *Earthq. Eng. Struct. Dyn.* **2015**, *45*, 5–27. [CrossRef]
5. Fisco, N.R.; Adeli, H. Smart structures: Part II—Hybrid control systems and control strategies. *Sci. Iran.* **2011**, *18*, 285–295. [CrossRef]
6. Alhan, C.; Sürmeli, M. Shear building representations of seismically isolated buildings. *Bull. Earthq. Eng.* **2011**, *9*, 1643–1671. [CrossRef]
7. Kelly, J.M. Aseismic base isolation: Review and bibliography. *Soil Dyn. Earthq. Eng.* **1986**, *5*, 202–216. [CrossRef]
8. Kelly, J.M. The role of damping in seismic isolation. *Earthq. Eng. Struct. Dyn.* **1999**, *28*, 3–20. [CrossRef]
9. Charmpis, D.C.; Phocas, M.C.; Komodromos, P. Optimized retrofit of multi-story buildings using seismic isolation at various elevations: Assessment for several earthquake excitations. *Bull. Earthq. Eng.* **2015**, *13*, 2745–2768. [CrossRef]
10. Charmpis, D.C.; Komodromos, P.; Phocas, M.C. Optimized earthquake response of multistorey buildings with seismic isolation at various elevations. *Earthq. Eng. Struct. Dyn.* **2012**, *41*, 2289–2310. [CrossRef]
11. Forcellini, D.; Kalfas, K.N. Inter-story seismic isolation for high-rise buildings. *Eng. Struct.* **2023**, *275*, 115175. [CrossRef]
12. Barbat, A.H.; Rodellar, J.; Ryan, E.P.; Molinares, N. Active Control of Nonlinear Base-Isolated Buildings. *J. Eng. Mech.* **1995**, *121*, 676–684. [CrossRef]
13. Tsai, H.C. The effect of tuned-mass dampers on the seismic response of base-isolated structures. *Int. J. Solids Struct.* **1995**, *32*, 1195–1210. [CrossRef]
14. Zheng, W.Z.; Wang, H.; Li, J.; Shen, H.J. Parametric study of SMA-based friction pendulum system for response control of bridges under near-fault ground motions. *J. Earthq. Eng.* **2021**, *25*, 1494–1512. [CrossRef]
15. Zheng, W.; Tan, P.; Liu, Y.; Wang, H.; Chen, H. Multi-stage superelastic variable stiffness pendulum isolation system for seismic response control of bridges under near-fault earthquakes. *Struct. Control Health Monit.* **2022**, *29*, e3114. [CrossRef]
16. Hochrainer, M.J.; Ziegler, F. Control of tall building vibrations by sealed tuned liquid column dampers. *Struct. Control Health Monit.* **2006**, *13*, 980–1002. [CrossRef]
17. Di Matteo, A.; Lo Iacono, F.; Navarra, G.; Pirrotta, A. Innovative modeling of Tuned Liquid Column Damper motion. *Commun. Nonlinear Sci. Numer. Simul.* **2015**, *23*, 229–244. [CrossRef]
18. Di Matteo, A.; Di Paola, M.; Pirrotta, A. Innovative modeling of tuned liquid column damper controlled structures. *Smart Struct. Syst.* **2016**, *18*, 117–138. [CrossRef]
19. Hochrainer, M.J. Tuned liquid column damper for structural control. *Acta Mech.* **2004**, *175*, 57–76. [CrossRef]

20. Bekdaş, G.; Nigdeli, S.M. Estimating optimum parameters of tuned mass dampers using harmony search. *Eng. Struct.* **2011**, *33*, 2716–2723. [CrossRef]
21. Bekdaş, G.; Nigdeli, S.M. Metaheuristic based optimization of tuned mass dampers under earthquake excitation by considering soil-structure interaction. *Soil Dyn. Earthq. Eng.* **2017**, *92*, 443–461. [CrossRef]
22. Nigdeli, S.M.; Bekdaş, G. Optimum tuned mass damper design in frequency domain for structures. *KSCE J. Civ. Eng.* **2016**, *21*, 912–922. [CrossRef]
23. Tena-Colunga, A.; Eduardo Pérez-Rocha, L.; Avilés, J.; Cordero-Macías, C. Seismic isolation of buildings for power stations considering soil-structure interaction effects. *J. Build. Eng.* **2015**, *4*, 21–40. [CrossRef]
24. Clemente, P.; Martelli, A. Seismically isolated buildings in Italy: State-of-the-art review and applications. *Soil Dyn. Earthq. Eng.* **2019**, *119*, 471–487. [CrossRef]
25. Alhan, C.; Öncü-Davas, S. Performance limits of seismically isolated buildings under near-field earthquakes. *Eng. Struct.* **2016**, *116*, 83–94. [CrossRef]
26. Alemdağ, E.C. A New Method to Increase Effectiveness of Base Isolation on Torsionally Unrestrained Structures. Master's Thesis, Middle East Technical University, Ankara, Turkey, 2016.
27. Hitchcock, P.A.; Kwok, K.C.S.; Watkins, R.D.; Samali, B. Characteristics of liquid column vibration absorbers (LCVA)—II. *Eng. Struct.* **1997**, *19*, 135–144. [CrossRef]
28. Huo, L.S.; Li, H.N. Structural vibration control using semi-active variable stiffness tuned liquid column damper. *J. Vib. Shock* **2012**, *31*, 157–164.
29. Ziegler, F. *Mechanics of Solids and Fluids*, 2nd ed.; Springer: New York, NY, USA, 1998.
30. Taniguchi, T.; Der Kiureghian, A.; Melkumyan, M. Effect of tuned mass damper on displacement demand of base-isolated structures. *Eng. Struct.* **2008**, *30*, 3478–3488. [CrossRef]
31. Lin, S.M. Nonlinear vibration control of a tall structure with tuned liquid column damper. *Mech. Adv. Mater. Struct.* **2015**, *23*, 146–155. [CrossRef]
32. Liu, G.H.; Li, H.N. An equivalent calculation method for analysis of structural vibration control of transforming TLD-structure to TMD-structure system. *Eng. Mech.* **2011**, *28*, 31–34.
33. Fu, C. Transforming Method of TLCD-structure to TMD-structure for Vibration Control. *KSCE J. Civ. Eng.* **2018**, *22*, 1384–1393. [CrossRef]
34. Di Matteo, A.; Furtmüller, T.; Adam, C.; Pirrotta, A. Optimal design of tuned liquid column dampers for seismic response control of base-isolated structures. *Acta Mech.* **2017**, *229*, 437–454. [CrossRef]
35. Rao, R. Jaya: A simple and new optimization algorithm for solving constrained and unconstrained optimization problems. *Int. J. Ind. Eng. Comput.* **2016**, *7*, 19–34. [CrossRef]
36. United States Federal Emergency Management Administration. *Quantification of Building Seismic Performance Factors*; FEMA P695; United States Federal Emergency Management Administration: Washington, DC, USA, 2009.
37. Yang, J.N.; Danielians, A.; Liu, S.C. Aseismic Hybrid Control Systems for Building Structures. *J. Eng. Mech.* **1991**, *117*, 836–853. [CrossRef]
38. Tributsch, A.; Adam, C. Evaluation and analytical approximation of Tuned Mass Damper performance in an earthquake environment. *Smart Struct. Syst.* **2012**, *10*, 155–179. [CrossRef]